Dear Editor and Reviewers,

Thank you very much for your letter and for the constructive and insightful comments concerning our manuscript, entitled **"Nascent Eocene Indian Monsoons recorded in oyster shells from the western Indian margin"** (Manuscript ID: **egusphere-2026-1393**).

We sincerely appreciate the time and effort you have dedicated to reviewing our work. Your thoughtful comments and suggestions have been extremely valuable in improving the clarity, scientific rigor, and overall quality of the manuscript. We have carefully considered all comments and have revised the manuscript accordingly.

We have addressed the three main concerns raised by the reviewers in the revised manuscript:

1. **Definition of threshold criteria for identifying pristine and potentially diagenetically altered shell zones**

We have added a dedicated section to the Methodology that defines the threshold values used to distinguish pristine shell material from zones that may have been affected by diagenetic alteration. This provides a clearer and more objective basis for the screening of the shell material.

2. Absence of a chronological age model and reliance on climate-model-based seasonal assignments

We have incorporated ShellChron-derived ontogenetic age models for both shells. This provides an independent chronological framework for the shell records and allows the seasonal interpretations to be evaluated within a shell-based temporal context, rather than relying solely on climate-model simulations.

3. Reliance on a single shell and potentially overambitious climatic interpretations

We have revised the analysis to include both pristine shells in the climatic reconstruction. Furthermore, we have substantially refined the interpretations and now base our conclusions primarily on the proxy-derived evidence, with the climate-model simulations used as supporting evidence rather than as the primary basis for interpretation. This has allowed us to moderate the interpretations and ensure that the conclusions remain consistent with the available proxy data.

Based on the interpretations in the revised manuscript, we have modified the title of the manuscript also. In the revised manuscript, the title is: "**Sustained high temperatures and seasonal hydroclimate variability recorded in the middle Eocene oyster shells from the tropical western Indian margin"**

In the detailed response document (attached), we have addressed the reviewers' concerns through additional clarification, revision of the text and figures, and improvements to the presentation and interpretation of our results. We believe that these revisions have substantially strengthened the manuscript.

Please find below our detailed, point-by-point responses to all comments.

For clarity,

Reviewers' comments are presented in blue

Authors' responses are presented in black

Changes made in the revised manuscript are presented in red.

We sincerely thank the Editor and Reviewers again for their constructive feedback and for the opportunity to improve our manuscript. We hope that the revised version satisfactorily addresses all of the concerns raised and will be suitable for publication.

Sincerely,
Aniket Mitra
On behalf of the authors.

REVIEWER 2:

Mitra et al. present in this manuscript a geochemical analysis of 3 fossil mollusc shells from the Bartonian Eocene formation in India to study paleoclimate seasonality and the onset of the monsoon in this region.

The study displays an impressive range of sophisticated analytical techniques, statistical treatments, comparison with climate simulation, and high-quality elaborated figures. They convincingly demonstrate the good preservation of 2 of the shells, which were selected for isotopic analyses.

However, I cannot recommend the publication of this work in its current state because of a major methodological flaw in determining the seasonal nature of shell isotopic variations, which means that past climate seasonality is not resolved in this proxy record, and that none of the discussion and conclusion regarding past climate seasonality is supported.

The problem appears in section 5.4.

So far, the authors have presented no information or evidence regarding the shell growth rate that could help to estimate the temporal resolution of the isotopic record, which is the key information to know the time scale of the observed variations.

Response: Thank you for your careful assessment of the manuscript and for pointing out this important limitation. In the revised manuscript, we have incorporated a shell-growth chronology model based on ShellChron (de Winter, 2022). The estimated temperatures, stable isotope ($\delta^{18}O_{cc}$ and $\delta^{13}C_{cc}$) variations, $\delta^{18}O_w$, and trace-element profiles are now evaluated within the relative monthly framework generated by the ShellChron-derived chronology. This provides a more robust temporal framework for interpreting the seasonal variations recorded in the shells.

Strangely the authors simply assume the seasonal time scale and chose to constrain the inner shell chronology using the most imprecise proxy record (four Δ47 data points) with a global Eocene paleoclimate simulation: "Clumped-isotope-derived SSTs can be compared to CESM simulated annual temperature variability to assign month-relative positions of the data points on the growth axis of [shell] K/Pk/02.", "This [shows] close consistency between the model results and the proxy based estimated values, and suggesting a minimum lifespan of ~2 years".

Response: In the revised manuscript, the four clumped isotope points are analysed based on the ShellChron derived age model of the oyster specimen K/PK/02. Please find below the methodology and results from ShellChron and the respective positions of the clumped isotope datapoints.

Lines 245-261:

3.9.2 Shell chronology

Shell chronology was estimated based on $\delta^{18}O_{cc}$ and trace element profiles along the growth axis of the resilifer of the shells, K/PK/01 and K/PK/02. K/PK/03 is excluded from the chronologic study, since we consider it diagenetically altered. We used the close correspondence between quasi-cyclic nature of large-ion lithophile elements (LILE: Sr, Ba) and REEs (La, Ce, Pr, Nd, Sm)/Ca (see Sections 4.3, 5.4) and $\delta^{18}O_{cc}$ variability as an indication that Sr/Ca captures seasonal variability in the pycnodont shells (as noted in de Winter et al., 2018). While the exact relationship between Sr/Ca ratios in molluscs and seasonal growth and temperature variability is poorly constrained (see e.g. Lorrain et al., 2005; Freitas et al., 2006), we interpret periodic variations in Sr/Ca coinciding with those in $\delta^{18}O_{cc}$ as the best approximation for seasonal growth.

Probable age markers along the oyster growth axes were identified using the well-established seasonal $\delta^{18}O_{cc}$ signal in conjunction with Sr/Ca cyclicity, where peaks of Sr/Ca come after the minimum values of $\delta^{18}O_{cc}$. A continuous, high-resolution (25 µm) Sr/Ca profile was incorporated into the ShellChron growth model (de Winter, 2022) to transform the trace-element records from distance to a seasonally constrained chronological domain. Because ShellChron can produce age inversions in high-resolution datasets, whereby a subsequent data point is assigned a younger age than its predecessor, the resulting age models were subsequently post-processed using a Monte Carlo approach following Han et al. (2026). This approach simulates shell growth through ontogeny while accounting for the uncertainty in the ShellChron output, thereby eliminating age inversions and generating a more realistic and continuous age model for complex datasets while remaining true to the seasonal growth rate distributions estimated by ShellChron.

Lines 355-362: The monthly resolved chronologies generated by ShellChron for the two best-preserved *Pycnodonte* shells, PK01 and PK02 record approximately 36 months of ontogenetic growth (Fig. 4). Resilifer accretion was broadly uniform, with ~5-7 mm of resilifer growth per year, corresponding to an estimated shell-length increment of ~44-64 mm/year (PK01: analysed resilifer 16 mm, shell height 142 mm; PK02: analysed resilifer 17 mm, shell height 156 mm). Distinct periods of reduced growth occur at months 0-6, 22-27, and 33-36 in PK01, and 0-2, 9-15, and 25-28 in PK02 (Fig. 4). As growth rate is not uniform, the 1-mm-spaced stable-isotope measurements results in uneven age spacing with an average of 5-7 measurements per year with a ~2 months resolution of analysis. The four robust clumped isotope temperature estimates, based on 9-11 replicates each correspond to months ~7, 16, 21 and 30 respectively according to the ontogenic age of the specimen PK02.

Lines 357-365:

The monthly resolved chronologies generated by ShellChron for the two best-preserved *Pycnodonte* shells, K/PK/01 and KPK/02 record approximately 36 months of ontogenetic growth (Figs. 4, S5). Resilifer accretion was broadly uniform, with ~5-7 mm of resilifer growth per year, corresponding to an estimated shell-length increment of ~44-64 mm/year (K/PK/01: analysed resilifer 16 mm, shell height 142 mm; K/PK/02: analysed resilifer 17 mm, shell height 156 mm). Distinct periods of reduced growth occur at months 0-6, 22-27, and 33-36 in K/PK/01, and 0-2, 9-15, and 25-28 in K/PK/02 (Fig. 4). As growth rate is not uniform, the 1-mm-spaced stable-isotope measurements results in uneven age spacing with an average of 5-7 measurements per year with a ~2 months resolution of analysis. The four robust clumped isotope temperature estimates, based on 9-11 replicates each correspond to months ~7, 16, 21 and 30 respectively according to the ontogenic age of the specimen K/PK/02 based on the growth rate model.

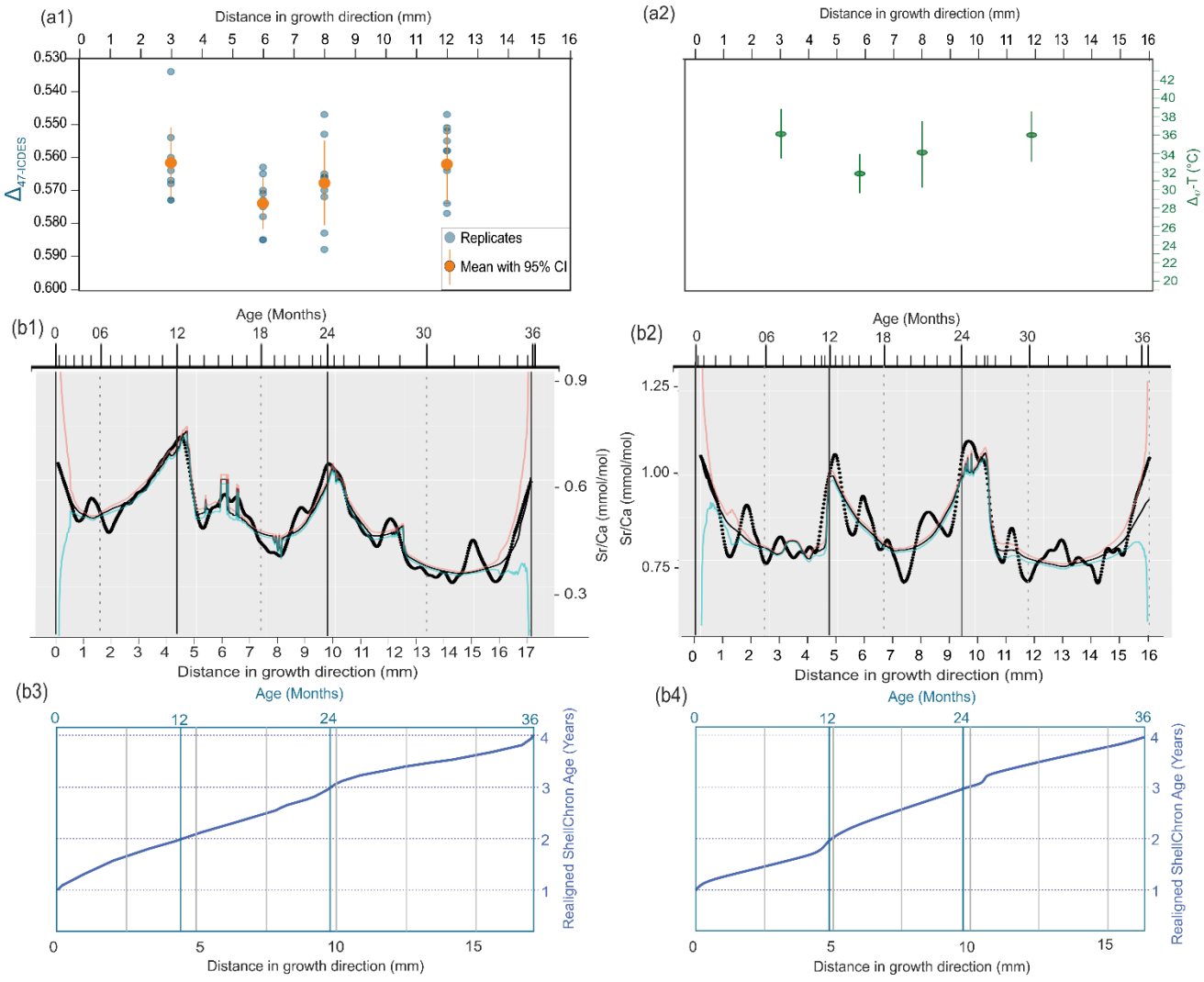

Figure 4. (a) Clumped ($\Delta_{47,\ \text{I-CDES}}$) isotope data: (a1) Average Δ_{47}, I-CDES with 95% CI in orange and all the measured individual replicates for the corresponding averages are plotted alongside the distance of shell resilifer growth profile of K/PK/02, (a2) resulting Δ_{47}-temperatures estimates are plotted along the growth profile of K/PK/02; (b) Chronologic shell growth of (b1) K/PK/01 and (b2) K/PK/02, as modelled by ShellChron (de Winter, 2022) based on the high resolution (25 µm) Sr/Ca profile recorded from the resilifer regions of the shells. Resulting age models were post-processed using a Monte Carlo approach for (b3) K/PK/01 and (b4) K/PK/02 following Han et al. (2026).

This is methodologically incorrect in many ways. It wildly assumes a data-model agreement on seasonality to create an internal chronology that validates the data-model agreement. And with only 4 datapoints with overlapping error bars. Without independent inner chronological indications, the variability between these 4 datapoints distributed over ~1 cm of growth could be intra-seasonal, interannual, decadal, or just the product of analytical uncertainty. The whole article is then built on the conclusion posing that these 4 datapoints represent seasonal extrema.

Response: Thank you for this helpful feedback. We derived the monthly assignments from the shell-growth chronology. Stable isotopes were measured at approximately 1 mm intervals. Although the ShellChron-derived age models for specimens K/PK/01 and K/PK/02 indicate variations in growth rate, they do not show major or systematic growth cessations or persistent periods of markedly slower or faster growth within individual years. Thus, the sampling resolution

corresponds to approximately two months (see **lines 357-365**). However, we fully agree with you that it is very difficult to estimate a precise growth rate based on various geochemical proxies in ancient shells from shallow sea environments in near coastal proximity. We see it more as the best possible approximation or approach to estimate growth rate of these extremely old organisms. It provides precise clumped isotope temperature estimates an anchor for the seasonality study of this former tropical environment. In future it might be possible to resolve it in more detail, but still the close similarity to the range of modern tropical seasonality and the few existing studies from tropical environments gives us confidence in our obtained results.

The clumped-isotope measurements were strategically collected from the highest and lowest $\delta^{18}O_{cc}$ values. As also noted in your later comments, the $\delta^{18}O_{cc}$ profiles capture a quasi-annual cycle. We therefore used these cycles to establish the age markers, supported by the corresponding Sr/Ca and Ba/Ca profiles, which exhibit similar quasi-cyclic patterns. Both specimens record approximately three annual cycles, as also recognised in your later comments.

Based on these annual markers, ShellChron (de Winter, 2022) generated shell-growth models at monthly resolution. The resulting age models were subsequently post-processed using a Monte Carlo approach following Han et al. (2026) (**lines 245-261**). We have therefore revised the manuscript to make clear that the monthly assignments are derived from the shell-based chronology rather than being imposed solely from the climate-model simulations.

The warmest clumped isotope temperature estimate was assigned to May, corresponding to the warmest month in both the modern observations and the Eocene CESM simulations. The remaining three measurements consequently fall within relatively warm and cool seasonal intervals. According to the age model, the first measurement corresponds to the first year, the second and third measurements to the second year, and the fourth measurement to the fourth year. Therefore, the temporal resolution of the clumped-isotope record is interannual to interseasonal, rather than monthly (lines 506–509).

Lines 506-509:

The estimated highest SST (Δ_{47}-T: $35.8^{+2.8}_{-2.7}$ °C; $\delta^{18}O_w$: $1.2^{+0.5}_{-0.5}$ ‰) point of month seven of K/PK/02 is aligned with May, the warmest month of a year, according to the modern Indian climatic scenario and CESM simulations of the Eocene (Fig. 7). Accordingly, the rest of the three clumped isotope temperature estimates from multiple replicates (9, 9 and 11 respectively) correspond to January-February (Δ_{47}-T: $31.3^{+2.2}_{-2.1}$°C; $\delta^{18}O_w$: $0.6^{+0.4}_{-0.4}$ ‰), June-July (Δ_{47}-T: $33.5^{+3.7}_{-3.6}$ °C; $\delta^{18}O_w$: $0.8^{+0.7}_{-0.7}$ ‰) and April-May (Δ_{47}-T: $35.6^{+3.0}_{-2.9}$ °C; $\delta^{18}O_w$: $1.6^{+0.6}_{-0.5}$ ‰). The observed range of temperature variation should be carefully interpreted as minimum seasonality estimates, due to the low sampling resolution required to obtain enough material for robust clumped isotope analysis.

Without a robust inner chronology, the discussion about the supposedly annual cyclicity of elements is also completely speculative. Affirming that their variations are "evidently" annual is an attempt of authoritative argument. First, the periodicity in elemental ratios doesn't match the proposed chronology: the authors conclude that the record is 2-years long while Sr/ca shows 4 peaks that could be interpreted as 3 "annual cycles". Elemental ratios in mollusc shells have never been demonstrated to be reliable paleoenvironmental indicators anyway. Relationships have been observed in some cases but are generally coincidental, not reproducible, suggesting that the environmental signal appears indirectly through a strong biological control (the biological control on elemental ratios, in particular growth rate, has been demonstrated in several species).

The authors need first to independently demonstrate the existence of climatic annual cycles in their record. Elemental ratios may follow annual cyclicity but the mechanisms of their incorporation is not stable enough for them to be used as primary indicators. Oxygen stable isotope ratio are, on the contrary, a physically controlled proxy, widely validated across all biocarbonate organisms.

Response: In the revised manuscript, we have developed an independent shell-growth chronology using ShellChron, as described in our earlier responses. Following your suggestion, we have used the quasi-cyclic variations in $\delta^{18}O_{cc}$ as the primary basis for identifying annual markers, with the corresponding Sr/Ca and Ba/Ca profiles used as supporting evidence. The four successive peaks observed in the elemental profiles therefore correspond to approximately three annual cycles within the shell-growth record.

We have also moderated our previous wording and no longer describe the elemental variations as "evidently" annual. Instead, we refer to them as quasi-cyclic variations that are consistent with the annual cyclicity identified from the $\delta^{18}O_{cc}$ record and clumped isotope derived temperature estimates. This distinction is important because we acknowledge that trace-element incorporation in molluscan shells can be influenced by environmental factors, including freshwater input, precipitation-evaporation balance, and productivity, as well as by biological and growth-related effects.

The close correspondence among the Sr/Ca, Ba/Ca, and La/Ca profiles, together with the recurrent occurrence of their peaks following minima in $\delta^{18}O_{cc}$, provides supporting evidence for a recurrent seasonal pattern. We have also added relevant published evidence demonstrating seasonal variations in Sr/Ca in fossil bivalves, including observations from Cretaceous *Pycnodonte*. These studies support the possibility of seasonally modulated trace-element incorporation, while we recognise that such relationships may be species- and environment-specific and can be affected by biological controls.

Lines 546-584:

Sr/Ca, Ba/Ca, La/Ca show seasonal variation with peaks corresponding to September-October. CESM simulations indicate that India experiences peak precipitation during these two months (Fig. 8; Baatsen et al., 2020). Although proxy based temperature- $\delta^{18}O_w$ values are unavailable for these intervals (September-October), the observed decline in reconstructed temperature and consistent $\delta^{18}O_w$ decrease from April to July with the model-simulated increase in precipitation (Fig. 8), providing independent support for the inferred seasonal hydroclimatic pattern. Sr incorporation in calcitic shells has been shown to increase with higher precipitation rates in inorganic calcite (Morse and Bender, 1990). Additionally, Eocene bivalves from North Sea records higher Sr and Ba during months of freshwater influx, as terrestrial run-offs contain much higher rate of these elements (Kniest et al., 2024). Increased Ba/Ca ratio is commonly associated with blooms of specific phytoplankton species (Goodwin et al., 2013; Poitevin et al., 2020; Fröhlich et al., 2022). The strong covariation between $\delta^{13}C_{cc}$ and Ba/Ca, with coincident maxima during inferred high-rainfall intervals, is consistent with enhanced primary productivity associated with seasonal terrestrial nutrient delivery associated with fresh-water influx (Goodwin et al., 2013). Similar rainfall-associated productivity increases have been documented in tropical and equatorial coastal lagoons (Herrera-Silveira, 1998; Soondur et al., 2021; Cutrim et al., 2026), supporting a potential link between seasonal runoff and phytoplankton productivity in the Eocene equatorial Kutch setting. Seasonal influences are evident, with peak concentrations of a few trace elements typically observed during the months of increased phytoplankton productivity and/or enhanced fluvial input enriched in trace metals (Liu et al., 2021). While REE incorporation is generally minimally affected by seasonality within a 5-20 °C range (Mouchi et al., 2020), the significantly higher temperatures (30-36 °C) during the late Bartonian India likely influenced REE uptake.

Because Na/Ca, Mg/Ca, and Cu/Ca in the K/PK/01 specimen show strong ontogenetic trends that may obscure seasonal variability, their incorporation mechanisms are beyond the scope of this study, as their clear variation is seen in only one specimen, K/PK/02. However, their quasi-cyclic patterns in K/PK/02 suggest a potential seasonal component, which we briefly interpret in light of published literatures. Mg/Ca profiles, commonly interpreted as a palaeotemperature proxy in oyster shells (Surge and Lohmann, 2008; Bougeois et al., 2014; Durham et al., 2017), shows multiple peaks within a year and does not strongly covary in the pycnodonts with seasonal temperature and/or hydroclimate dynamics based on our conventional stable and clumped isotope analyses (Fig. 7). Its antiphase relationship with the Sr/Ca shows a pattern but failing to strictly follow the temperature dynamics and respective months proves that it is affected by salinity, water Mg/Ca ratio, growth, metabolism, and ontogeny (Putten et al., 2000; Schöne et al., 2010; Freitas et al., 2009; Mouchi et al., 2013). This highlights Mg/Ca profiles limitations in restricted, evaporative or freshwater-influenced environments (Tynan et al., 2017). The Na/Ca ratio in bivalve shells has been used as a palaeosalinity proxy (Golan et al., 2016; Higuera-Ruiz and Elorza, 2009), although its environmental signal can be substantially modulated by growth dynamics (Marali et al., 2017; Arndt et al., 2023), consistent with the latter mechanism observed in our record of K/PK/01. Transition metals such as Cu are incorporated into shells from suspended and dissolved phases, modulated by physiology and environment (Huanxin et al., 2000). Because Cu uptake into oyster shells is generally favoured in lower salinity conditions (Huanxin et al., 2000), we interpret elevated Cu/Ca ratios to elevated palaeo-rainfall for monsoon and post-monsoon months (Fig. 7).

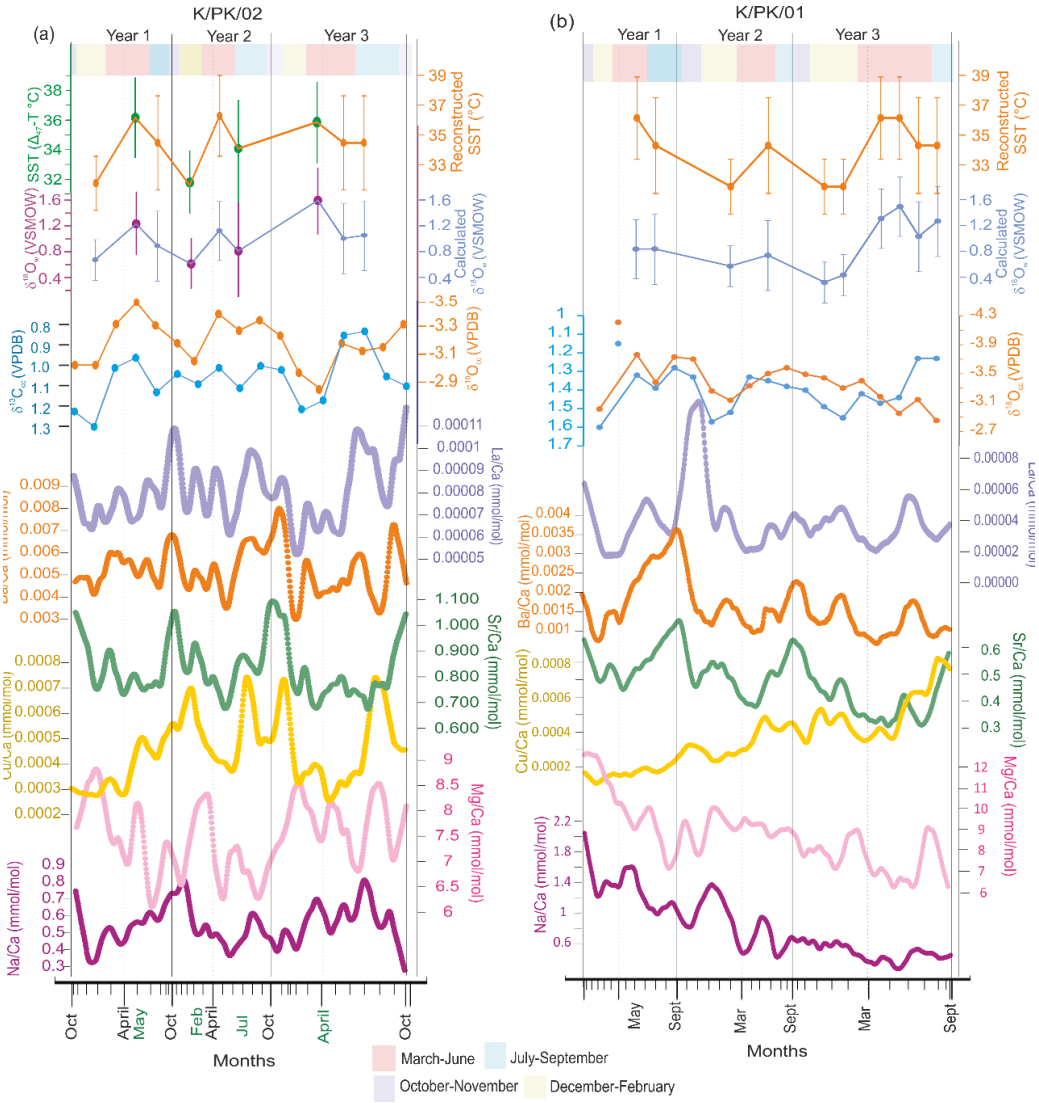

Figure 7. Trace element-to-Ca ratio profiles smoothened (LOWESS interval 0.1) along the growth axis of K/PK/02 and K/PK/01 are plotted together along the growth axis along with shell-chronology and stable isotope data, estimated Δ_{47}-T (red dots with 95% CI) and $\delta^{18}O_w$ (violet dots with 95% CI) values. Clumped isotope derived temperature estimates for the respective months along the shell chronology of K/PK/02 and K/PK/01 are shown as orange dots with 95% CI, with the corresponding calculated $\delta^{18}O_w$ ($f(\Delta_{47}\text{-}T, \delta^{18}O_{cc})$) values shown as blue dots.

δ18O records, which are generally used to infer annual cyclicity in mollusc shells, do not yield clear information here because of the shortness of the records (16 data points in one shell, and 18 in the other) and because of the coarse 1mm resolution of the analytic profiles. Yet, the micromilling technique used for the microsampling allows for extremely high resolution. Isotopic records in shells are now commonly achieved with 0.1mm spatial resolution.

To obtain useful information from these shells, the authors need to resample them in much higher resolution for $\delta^{18}O$ analyses to test whether the assumed annual cyclicity is robustly defined. If annual cycles do appear in the $\delta^{18}O$ record, those should be used to define seasons and an inner chronology. Only then, samples known to represent seasonal extrema should be collected for Δ47 temperature and δ^{18}Ow estimates.

Response: Thank you for this constructive comment. We agree that higher-resolution $\delta^{18}O_{cc}$ sampling would provide a stronger basis for resolving annual cyclicity. We acknowledge that the approximately 1 mm sampling interval used in this study is coarser than the spatial resolution achievable with modern micromilling techniques. But the oxygen isotope record, generated at approximately 1 mm sampling resolution, already reveals clear and coherent trends, with no evidence of substantial scatter attributable to insufficient growth resolution. Therefore, for the analysed fossils, increasing the sampling resolution would likely not provide substantially clearer information. If major changes in growth rate or seasonal variability were being missed, we would expect to observe more abrupt shifts or excursions at the scale of individual sampling points, rather than the relatively gradual changes observed in our record. However, the sampling resolution was constrained by the preservation and geometry of the shell material, as detailed below.

1) The shell material becomes particularly brittle toward the edge of the resilifer, making high-resolution and closely spaced micro-sampling difficult without risking fragmentation or loss of the pristine shell material.

2) The best-preserved, pristine calcite occurs within a relatively thin region of approximately 1-2 mm near the resilifer edge (**lines 372-380**). We therefore restricted the stable-isotope sampling to this thin preserved zone.

3) deeper drilling was avoided because the resilifer growth increments are curved rather than planar. Sampling deeper into the shell could therefore intersect adjacent growth layers and potentially mix material representing different stages of shell formation. Consequently, we restricted the stable-isotope sampling to the outermost approximately 1 mm of the preserved shell surface (reference to Figure 2).

These preservation-related constraints limited the amount of powder that could be obtained from each sampling position to approximately 100-150 µg. Within these constraints, we obtained 17 stable-isotope samples across the 16 mm resilifer of K/PK/02 and 19 samples across the 17 mm resilifer of K/PK/01, corresponding to an approximately 1 mm spatial sampling interval and an estimated temporal resolution of about two months based on the revised ShellChron-derived growth models **(lines 353-360)**.

For the Δ_{47} analyses, we necessarily sampled deeper into the shell because substantially larger amounts of material were required. This introduced a possibility of incorporating material from neighbouring growth layers and probably a slight dampening effect in case of sharp temperature excursions. However, the clumped isotope analyses require larger amounts of material than conventional oxygen isotope analyses, we tried to keep the required amount low with roughly a total of 5 mg including 9-11 replicates, to still obtain a robust temperature estimate and still, minimize the influence of spatial mixing (reference to table 3 and figure 4). The obtained seasonality based on the clumped isotope analyses has to be seen as minimum seasonality estimate and we have explicitly acknowledged this limitation in the revised manuscript, including the potential influence of the neighbouring low $\delta^{18}O_{cc}$ value on the fourth clumped-isotope measurement (lines 520-522).

We agree that resampling the shells at a substantially higher spatial resolution would be desirable. However, after the original sampling, the available pristine calcite in the relevant resilifer region has been largely consumed, and further high-resolution sampling is therefore no longer possible without compromising the remaining material. Given these constraints, we have revised the manuscript to avoid presenting the $\delta^{18}O_{cc}$ profiles as definitive records of annual cyclicity. Instead, the revised interpretation treats the observed $\delta^{18}O_{cc}$ quasi-cyclicity as supporting evidence within the ShellChron-derived chronology, with the associated uncertainties explicitly acknowledged.

Lines 376-380:

The pycnodonts are composed of two types of calcite crystals: foliated calcite, which forms the inner surface (i.e., cross-sectional edge: transect 1) of the resilifer and extends inward as thin channels (Figs. 2d-f, 3); and vesicular calcite, which occupies a larger portion of the shell interior as the oyster grows but is nearly absent near the resilifer edges (Fig. 2). The honeycomb-like vesicular calcite in pycnodonts is more prone to diagenetic alteration, as indicated by higher Fe incorporation, due to its porous structure compared to the more compact foliated calcite (Figs. 2-3; de Winter et al., 2018). The transect away from the resilifer edge contains higher concentration of Mn and Fe in a wider zone with respect to the edge, which is observed in all the specimens (Fig. 3). The area closest to the resilifer margin in pycnodonts contains the most pristine calcite, making it ideal for sclerochronological analysis due to its dominance of well-preserved foliated calcite. Thus, conventional oxygen and carbon isotope sampling is done from the resilifer edge.

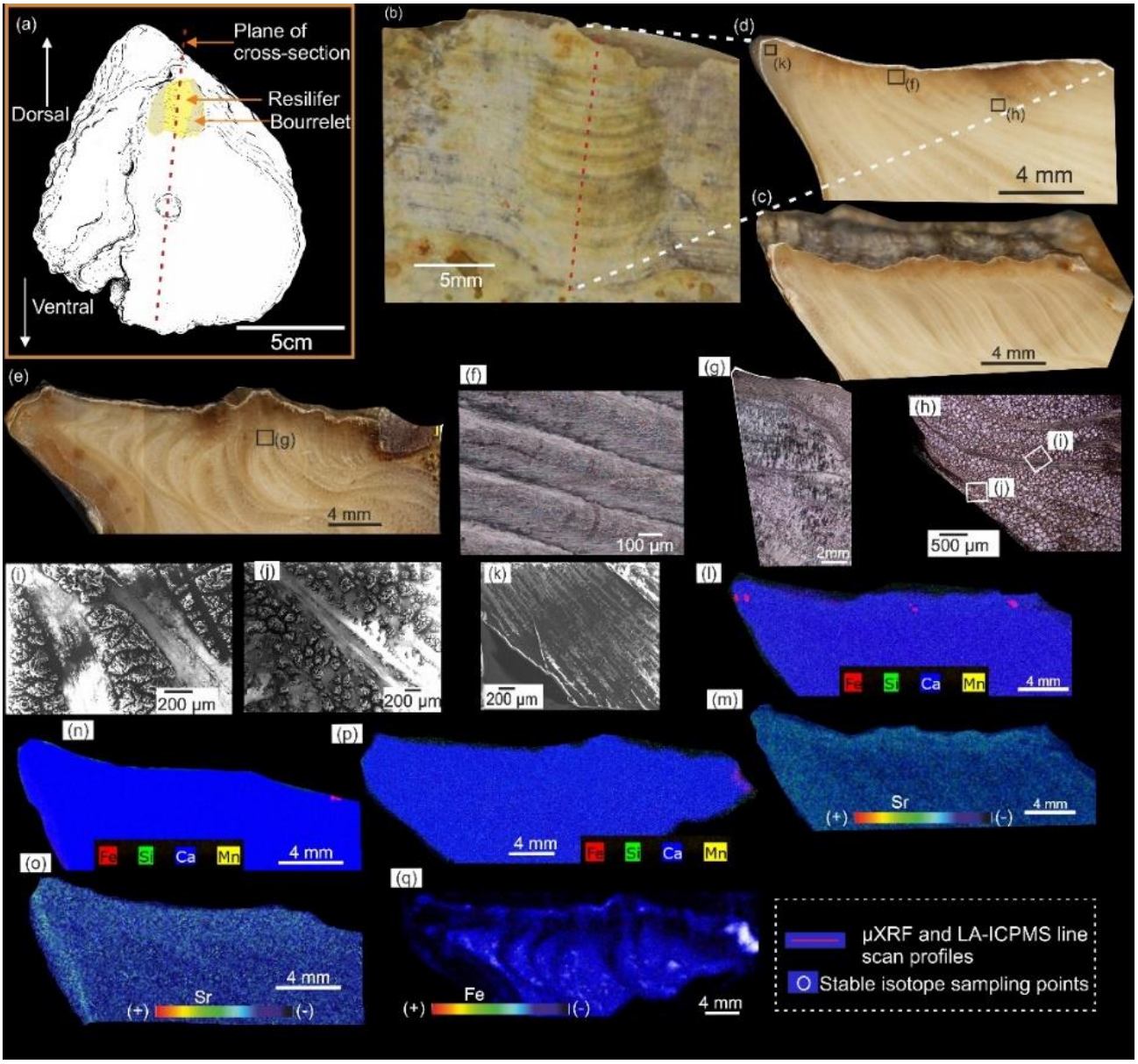

Figure 2. (a) Schematic diagram of *Pycnodonte kachchhensis* with plane of cross-section marked by dashed red line; Resilifer and bourlette makes the ligamental zone; (b) analysed ligamental region of K/PK/02; (c-e) Cross-sectional photograph of the shell resilifers: (c) K/Pk/01 (d) K/Pk/02 and (e) K/Pk/03; (f-h) Thin section microscopic images: (f) Foliated calcite from the resilifer zone of K/Pk/02; (g-h) Foliated and vesicular calcite in (g) K/Pk/03 and (h) K/Pk/02; (i-k) SEM images of foliated and vesicular calcite zones from K/Pk/02; (l-q) µXRF scanning maps of (l, n, p) Ca, Si, Mn and Fe (colour coded) and (m, o, r) elemental heat map of (i,m) K/Pk/01, (n,o) K/Pk/02 and (p,q) K/Pk/03.

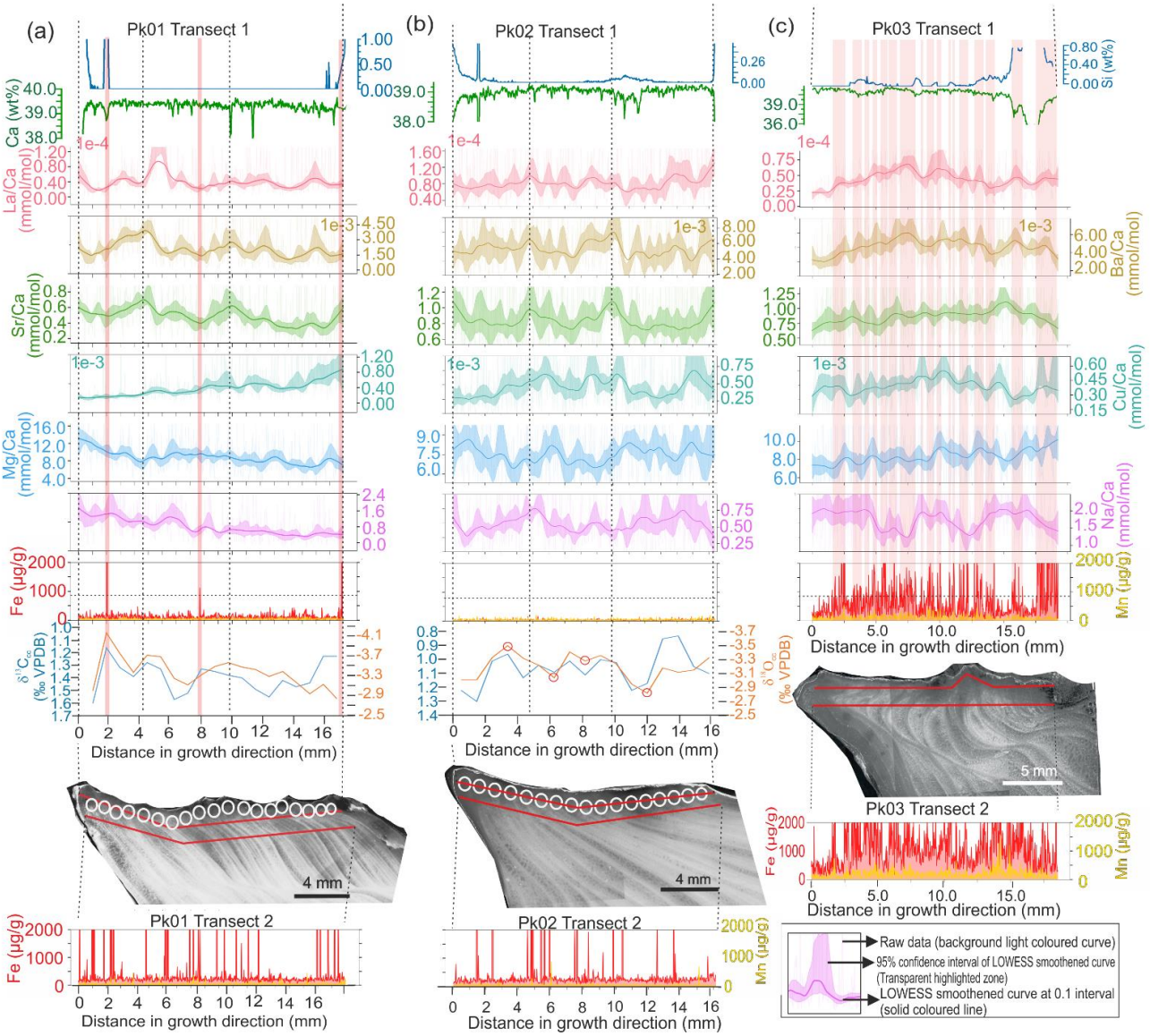

Figure 3. Plots of Ca and Si wt%, manganese (Mn) and iron (Fe) concentrations along with trace element-to-calcium ratios, measured along the growth axes of the resilifers in *P. kachchhensis* shells from resilifer edge transects of (a) K/PK/01 (b) K/PK/02 and (c) K/PK/03; and Mn, Fe concentrations from transects 2mm away from the resilifer edges at the bottom of the respective specimens. Red circles on $\delta^{18}O_{cc}$ profile of K/PK/02 indicate clumped isotope analyses points. Dotted vertical lines are indicative of probable year-markers. The line scan profiles are plotted on the cross-section image by red lines; white circles indicate stable isotope sampling points. Representative trace element-to-calcium ratio profiles from each element category (light metal, large ion lithophile elements, transition metals and rare earth elements) are shown. All trace element-to-calcium profiles is shown in supplementary file Fig. S4.

Distance (mm)	$\delta^{13}C_{cc}$ VPDB (‰)	$\delta^{18}O_{cc}$ VPDB (‰)	$\delta^{18}O_{cc}$ VSMOW (‰)	$\Delta_{47,\ I\text{-}CDES}$	Δ_{47}-T (°C)	$\delta^{18}O_w$ VSMOW (‰)	No. of replicates
3	0.87±0.04	-3.26±0.1	27.56±0.11	0.562±0.007	$35.8^{+2.8}_{-2.7}$	$1.2^{+0.5}_{-0.5}$	11
6	0.81±0.03	-3.04±0.06	27.79±0.07	0.574±0.006	$31.3^{+2.2}_{-2.1}$	$0.6^{+0.4}_{-0.4}$	9
8	0.79±0.03	-3.24±0.06	27.58±0.06	0.568±0.010	$33.5^{+3.7}_{-3.6}$	$0.8^{+0.7}_{-0.7}$	9
12	0.89±0.02	-2.84±0.03	27.99±0.03	0.562±0.008	$35.6^{+3.0}_{-2.9}$	$1.6^{+0.6}_{-0.5}$	11

Table 3. Clumped isotope results with estimated temperature (Δ_{47}-T) and $\delta^{18}O_w$ from specimen K/Pk/02. D_{47}-T calculated with temperature relationship of Anderson et al., 2021; $d^{18}O_w$ with temperature relationship of Kim and O'Neil, 1997; displayed uncertainties are 95% CI.

Even so, a 2-yr shell influenced by local lagoon conditions cannot be considered as representative of million-year scale continental climatology. Which means that more shells would need to be analysed to get at least some sampling of decadal to millennial variability and a meaningful estimate of mean conditions.

Response: Thank you for this important comment. We completely agree with your observation. We have therefore substantially revised the chronology, interpretation, discussion, conclusions, and abstract to ensure that the scope of our conclusions is consistent with the temporal and spatial limitations of our dataset.

With the ShellChron-derived chronology, the two shells each represent approximately three years of their recorded lifespan. We do not claim that these records represent long-term climate conditions over the Eocene or provide a reconstruction of monsoon variability over geological timescales. Rather, our objective in the revised manuscript is to characterise the seasonal to interannual environmental variability recorded by these two well-preserved shells during their growth, using an integrated multiproxy approach.

Both pristine shells are now included in the climatic reconstruction. The four clumped isotope temperature estimates based on 9-11 replicates each are used as robust temperature anchors to assign their corresponding positions within the shell-growth chronology. Stable-isotope measurements corresponding to the same chronological positions are then used to estimate $\delta^{18}O_w$, resulting in 19 paired temperature-$\delta^{18}O_w$ observations across the two shells. These data are complemented by trace-element profiles measured at approximately 25 µm spatial resolution over the three-year growth intervals.

Accordingly, our revised conclusions are based on the observed multiproxy variability within the shells, rather than extrapolating these records to represent million-year-scale continental climatology. The CESM simulations are used only as a climatic framework for evaluating whether the reconstructed seasonal patterns are physically plausible, rather than as a basis for extending our observations beyond the duration of the shell records.

Lines 684-702:

6 Conclusions

Well-preserved *Pycnodonte* shells successfully preserve the seasonal Eocene climate and environmental variability. The Kutch Basin's palaeo-equatorial climate during the late Bartonian is characterised by persistent warm temperature (~29-36 °C), with a shift towards evaporative conditions relative to the early Bartonian, demonstrating remarkable temperature stability despite the major Eocene climate events. This stable, warm climate, coupled with Tethyan Carbonate Ramp expansion, fostered formation of lagoon with the *Alveolina* wackestone at the basal Fulra Limestone. The basin's environmental evolution, from an early Bartonian shallow shelf with open marine and fluvial influence to a late Bartonian semi-restricted lagoonal setting, is reflected in lower amount of trace element signatures of the oyster shells and exceptionally higher $\delta^{18}O_w$ ($0.6^{+0.4}_{-0.4}$ and $1.6^{+0.6}_{-0.5}$ ‰) with respect to the Bartonian marine water (0 to -1.0 ‰).

Proxy-based reconstruction from the multi-year archive of the pycnodont shells, supported by climate model simulations, reveal small seasonal temperature difference (ΔSST: ~5 °C: 31-36 °C) comparable to modern north India (ΔSST: ~7 °C: 23-30 °C). The region likely maintained generally more extreme sea-surface temperatures than the present Gulf of Kutch,

with rainfall-driven cooling events associated with typical reduced evaporation for at least twice a year with a gap of ~7-8 months. Rainfall occurring ~8-9 months after peak summer had been facilitated by the advection of moisture from the open Tethys Seaway between India and Eurasia. Although the limited sampling points with large material requirements for robust Δ_{47}-temperature estimates do not permit reconstruction of the complete seasonal and the monsoon structure, but represent minimum seasonality. However, the identification of lower $\delta^{18}O_w$ during ~1-2 and ~8-9 months after peak summer provides evidence for a seasonally structured hydrological cycle in the late Bartonian India, different in character from modern four month confined summer monsoon of north India.

We have included all the new references in the revised manuscript following the in-text citations.